

Physical networks as network-of-networks

Gábor Pete,^{1,2,*} Ádám Timár,^{1,3} Sigurdur Örn Stefánsson,³ Ivan Bonamassa,⁴ and Márton Pósfai^{4,†}

¹*Alfréd Rényi Institute of Mathematics, Budapest, Hungary*

²*Budapest University of Technology and Economics, Budapest, Hungary*

³*University of Iceland, Reykjavík, Iceland*

⁴*Department of Network and Data Science, Central European University, Vienna, Austria*

(Dated: June 14, 2024)

Physical networks are made of nodes and links that are physical objects embedded in a geometric space. Understanding how the mutual volume exclusion between these elements affects the structure and function of physical networks calls for a suitable generalization of network theory. Here, we introduce a network-of-networks framework where we describe the shape of each extended physical node as a network embedded in space and these networks are bound together by physical links. Relying on this representation, we introduce a minimal model of network growth and we show for a general class of physical networks that volume exclusion induces heterogeneity in both node volume and degree, with the two becoming correlated. These emergent properties strongly affect the dynamics on physical networks: by calculating their Laplacian spectrum as a function of the coupling strength between the nodes we show that degree-volume correlations suppress the role of hubs as early spreaders in diffusive dynamics. We apply the network-of-networks framework to describe several real systems and find properties analog to the minimal model networks. The prevalence of these properties points towards general growth mechanisms that do not depend on the specifics of the systems.

INTRODUCTION

The building blocks of physical networks are extended objects that do not intersect each other, resulting in non-trivial geometric layouts [1], link entanglement [2] and emergent correlations between physical and network structure [3]. Yet, these works model nodes as localized spheres connected by extended tube-like links, an assumption that does not necessarily reflect the structure of most real-world physical networks. In the connectome, for example, nodes represent neurons with non-trivial dendritic shapes and links are point-like synapses [4]. A similar picture emerges for molecular networks such as the cytoskeleton, mitochondrial networks or fiber materials, where nodes are extended molecular strands and bonds between them are localized [5–7], as well as in the wood-wide-web, where extended tree roots and mycelia connect to form a complex underground network [8, 9]. Therefore, the sphere-tube paradigm often falls short at describing physical networks, calling for a more general framework to cope with the complex shape of nodes and links.

In this work we develop a network-of-networks representation of physical networks that is able to capture arbitrary node shapes [10, 11] and allows us to characterize both structural and dynamical properties of networks. Relying on the network-of-networks framework, we introduce a model that grows physical networks from fractal segments. Analytically solving the model, we show

that physicality induces heterogeneity in both the physical and the network properties of the nodes and that the two become strongly correlated. These correlations also affect the dynamics on the networks: generalizing the combinatorial Laplacian to physical networks [12–14], we show that fast dynamical modes associated to hubs (and corresponding to the tail of the Laplacian spectra) are suppressed by the emergent correlations between node volume and degree. The usefulness of the mathematical tools we develop in this paper go beyond the specifics of the model, and we demonstrate this by applying our framework to several real physical networks, including a recently collected data set describing more than $\sim 20,000$ neurons of the adult fruit fly’s brain [15]. In doing so, we identify positive node degree-volume correlations similar to our minimal growth model, and we show that these have an analog effect on the Laplacian spectrum of the connectome. The fact that degree-volume correlations emerge in a minimal model while also prevalent in real systems suggests a general mechanism behind such correlations that does not depend on the complex details of the growth of real networks.

RESULTS

Network-of-networks representation

We aim to describe physical networks embedded in some substrate or medium. In its most general form, the substrate is represented by a graph \mathcal{S} , and each physical node i is an extended object occupying a subgraph $\mathcal{V}_i \subset \mathcal{S}$. To capture volume exclusion, we do not allow nodes to overlap, i.e., $\mathcal{V}_i \cap \mathcal{V}_j = \emptyset$ for $i \neq j$. Two

* gabor.pete@renyi.hu

† posfaim@ceu.edu

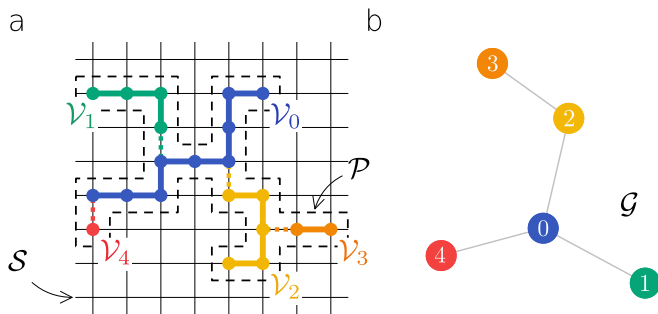


FIG. 1. **Network-of-networks representation.** (a) Each physical node \mathcal{V}_i is a subgraph of the substrate \mathcal{S} . Physical nodes cannot overlap, i.e., $\mathcal{V}_i \cap \mathcal{V}_j = \emptyset$ for $i \neq j$. The physical layout \mathcal{P} (dashed area) is a network-of-networks: it is the union of physical nodes \mathcal{V}_i together with the bonds connecting them. (b) The combinatorial network \mathcal{G} is a coarse-grained representation of \mathcal{P} capturing the connections between the nodes without the physical structure.

nodes i and j may form a link (i, j) if they occupy adjacent sites in \mathcal{S} . The physical layout \mathcal{P} of the network is a network-of-networks, i.e., it is the union of physical nodes, where each node is a network itself, together with the bonds forming the connections between the nodes (Fig. 1a). The layout \mathcal{P} is a physical realization of the combinatorial network \mathcal{G} , where node i of \mathcal{G} corresponds to the physical node \mathcal{V}_i , and nodes i and j are connected if there is a bond between \mathcal{V}_i and \mathcal{V}_j in \mathcal{P} (Fig. 1b). Though the substrate \mathcal{S} can represent any available space, here we focus on substrates that are d dimensional cubic lattices with linear size L and periodic boundary conditions. Note that network representations of this kind are employed in the graph drawing literature with the focus on algorithms that embed a given combinatorial network into \mathcal{S} [16]. Here, we are interested in physical networks \mathcal{P} growing in \mathcal{S} , the emergent relation between \mathcal{P} and \mathcal{G} , and its consequences on the dynamics on the network.

Network growth

To study the effect of physicality on network evolution, we define a model of network growth relying on the network-of-networks representation. We start with an empty \mathcal{S} and we place a single physical node \mathcal{V}_0 occupying a subset of the sites. We add the rest of the nodes iteratively: At time step t we add a new node \mathcal{V}_t that is seeded at a random unoccupied site and grows until it hits an already existing node \mathcal{V}_s and a link $(t-s)$ is formed. The growth of node \mathcal{V}_t is driven by some random or deterministic process; and we assume that the physical nodes are characterized by a fractal dimension $d_f \in [1, d]$ [17, 18]. We add N physical nodes or until all of \mathcal{S} is occupied; in the latter case we call the physical network saturated.

Since the total volume of the network increases over time, later nodes hit the network at higher rates and the typical size of nodes decreases. Hence, we expect that nodes added early have higher degree than nodes added in the final stages of the network evolution, both because they are larger and they have more time to collect connections. This suggests that to analytically characterize the evolution of the physical network two ingredients have to be considered: (i) network growth, i.e., nodes are added sequentially to the system and (ii) externally limited node growth, i.e., the nodes grow until they hit the already existing network. We show that these two ingredients lead to the emergence of power law combinatorial networks with degree exponents $\gamma \leq 3$.

We start the analytical treatment of the model by estimating the probability p_{ij} that two randomly placed physical nodes \mathcal{V}_i and \mathcal{V}_j intersect. If the two boxes containing the physical nodes have side length $l_i \gg l_j$, respectively, and the larger node \mathcal{V}_i intersects the box containing the smaller node \mathcal{V}_j , then, by dimension count, the two nodes overlap with positive probability if $d_f \geq d/2$. We can tile the lattice with $(L/l_j)^d$ boxes with side length l_j , and the number of such boxes intersected by \mathcal{V}_i is $\sim (l_i/l_j)^{d_f}$. Therefore the intersection probability is

$$p_{ij} \sim \frac{l_i^{d_f} l_j^{d-d_f}}{L^d} \sim \frac{v_i v_j^{d/d_f-1}}{L^d}, \quad (1)$$

where $v_i = |\mathcal{V}_i| \sim l_i^{d_f}$ is the volume of node i . If, however, $d_f < d/2$ and $l_j \leq l_i \ll L$, then the nodes avoid each other with high probability. In this case, the intersection probability will have the meanfield behavior, well-approximated by the probability of selecting the sites of \mathcal{V}_i and \mathcal{V}_j uniformly from \mathcal{S} , i.e., $p_{ij}^{\text{MF}} \sim v_i v_j / L^d$, which is independent of d_f and agrees with Eq. (1) for $d_f = d/2$.

Using the same box-counting argument that led to Eq. (1), the probability that a node added at time t intersects any existing node $s < t$ is approximately given by $\sum_{s < t} p_{st} = v_t^{d/d_f-1} V_{t-1} / L^d$, where V_{t-1} is the total volume of nodes $s < t$. A key observation is that the size of node t increases until it hits the existing network, meaning that v_t increases until $\sum_{s < t} p_{st} \approx 1$, allowing us to estimate the volume of node t as

$$v_t \approx (V_{t-1} / L^d)^{-\frac{d_f}{d-d_f}}. \quad (2)$$

Equation (2) allows us to express the evolution of the expected total volume via the recursion $V_{t+1} = v_{t+1} + V_t$ with initial condition $V_0 = v_0$. Using a continuous time approximation, we obtain

$$V_t \approx L^d \left[\frac{d}{d-d_f} \frac{t+c}{L^d} \right]^{\frac{d-d_f}{d}} \sim L^d \left(\frac{t}{L^d} \right)^{1-d_f/d}, \quad (3)$$

where c is a constant depending on v_0 . A natural choice for the latter is that the first node spans the entire available space, i.e., $v_0 \sim L^{d_f}$, in which case c is independent

of L . Equation (3) predicts that N_{sat} , the number of nodes when the network saturates, scales as $N_{\text{sat}} \sim L^d$, meaning that the average node volume $\langle v \rangle$ remains constant in the $L \rightarrow \infty$ large system limit. Therefore, the physical layout \mathcal{P} is optimal in the sense that no physical representation of a combinatorial network of N_{sat} nodes can fit into a smaller volume than $\sim N_{\text{sat}} \sim L^d$. It is noteworthy that the model achieves this bound despite the fact that the nodes grow randomly.

In light of Eq. (3), we can now calculate the expected degree of the physical nodes in the combinatorial network \mathcal{G} . In the continuous time approximation, the volume of the newly added node v_t is provided by the time derivative of V_t , i.e., $v_t \sim (t/L^d)^{-d_t/d}$. Hence, following Eq. (1), the expected degree of node t after the addition of N nodes is

$$k_t(N) = 1 + \frac{v_t}{L^d} \sum_{s=t+1}^N v_s^{d/d_t-1} \sim v_t \cdot \left(\frac{N}{L^d} \right)^{\frac{d}{d_t}}, \quad (4)$$

where the proportionality is valid for $t \ll N$. This means that the volume occupied by large nodes (i.e., nodes that were added early) in the physical layout is proportional to their degree in the combinatorial network.

We finally calculate the complementary cumulative degree distribution $P(k) = 1 - \frac{1}{N} \sum_{t:k_t \geq k}^N 1$, finding that $P(k) \sim k^{-(\gamma-1)}$ with exponent

$$\gamma = 1 + \frac{d}{d_f}. \quad (5)$$

For $d_f \leq d < 2d_f$ the degree exponent falls in the range $2 \leq \gamma < 3$. In the mean-field regime the degree exponent can be obtained by substituting d/d_f with 2, yielding $\gamma_{\text{MF}} = 3$. Note that the upper critical dimension of the physical network depends on the kinetic growth of the nodes. For example, growing nodes along a straight trajectory in a random direction generates nodes with $d_f = 1$; therefore the networks fall in the mean-field regime $d_f \leq d/2$ even for embedding dimension $d = 2$.

In the above model, each physical node grows starting from a random location following some growth process. We stress that our calculations hold for a general class of node growth algorithms, the crucial assumption being that if the boxes around two random walk pieces intersect, then with uniformly positive probability the trajectories also intersect, which implies a level of isotropy of node growth. As a counterexample, consider nodes that always grow in one direction along one of the axes. Such nodes will run parallel to each other, avoiding intersection, hence the resulting network will be a collection of disconnected chains. If, however, the nodes grow along straight lines but in random directions, thus restoring isotropy on average, then the resulting network has a power law degree distribution (SI Sec. S1.4).

Numerical simulations

To test our analytical predictions, we numerically generate physical networks where nodes grow according to random walk trajectories. Specifically, we generate nodes using loop-erased random walks (LERWs), i.e., a trajectory that evolves as a simple random walk in which any loop is erased as soon as it is formed [19–22]. Here, we focus on the LERW, as it represents a tractable model of non-self-intersecting random trajectories with well-understood non-trivial critical properties. Its critical properties are studied both in the mathematics and physics literature [23–26]; for example, their fractal dimension in $d = 2$ is $d_f = 5/4$ [22], in $d = 3$ it is $d_f \simeq 1.6236(4)$ [27, 28], while its upper critical dimension is $d_u = 4$ where $d_f = 2$ with a logarithmic correction [29]. (See METHODS for further details.) We remark that our predictions are not specific to LERWs, in Sec. S1 of the Supplementary Information we study various alternative growth processes.

Knowing the fractal dimensions of LERWs allows us to directly verify the predictions of Eqs. (3)–(5):

Volume evolution. Equation (3) predicts that the total volume of the physical network evolves as $V_t \sim t^{1-d_f/d}$. Figure 2a shows the excellent agreement between the theoretical predictions and numerical simulations. Note that, as expected, in the mean-field regime $d \geq 4$ the network volume follows the classic diffusion growth $V_t \sim t^{1/2}$. Figure 2b further corroborates the predicted scaling of the number of nodes at saturation, i.e., $N_{\text{sat}} \sim L^d$.

Degree-volume correlations. A second prediction is the emergence of degree-volume correlations, capturing the interplay between the physical layout \mathcal{P} and the combinatorial network \mathcal{G} . In particular, Eq. (4) predicts a linear proportionality between the node volume v_i and degree k_i , and we again find excellent agreement with simulations for all the tested dimensions (Fig. 2c).

Power law emergence. As a final test, we verify the emergence of power law scaling in the degree distribution of the combinatorial networks \mathcal{G} . As anticipated in Eq. (5), the degree exponent depends on both the dimensionality of the embedding substrate, d , and the fractal dimension of the nodes, d_f . Figure 2d shows that numerical simulations confirm the predicted degree exponent $\gamma = 1 + d/d_f$ for dimensions $d < 4$, while the mean-field exponent $\gamma_{\text{MF}} = 3$ is found for $d \geq 4$. In traditional models of combinatorial networks, heterogeneity typically arises from preferential attachment or some other optimization process. Our model is based on random growth without any explicit preference to create highly connected nodes; therefore, the uniform attachment tree may be considered as the non-physical counterpart of our model. Uniform attachment yields exponential degree distribution, hence the power law distribution observed

here is a direct consequence of volume exclusion, which, together with the dynamic network growth, induces effective preferential attachment.

Physical network Laplacian

The layout \mathcal{P} is a physical realization of the combinatorial network \mathcal{G} . Traditional studies of dynamics on physical networks ignore the layout \mathcal{P} and focus only on the role of \mathcal{G} , thus prompting the question: does modeling dynamics on \mathcal{G} accurately capture dynamics on physical networks? To explore this, we study the spectral properties of \mathcal{P} and show that physical nodes emerge as functional units through timescale separation, yet even in this limit the structure of \mathcal{P} continues to affect the dynamics. We focus on the Laplacian spectrum [12] since it influences the behavior of several dynamical processes on networks [30] including diffusion [31, 32], synchronization [33] and it underlies the definition of several information-theoretic tools to analyze the multiscale functioning of networks [10, 14, 34–37].

We study the problem by invoking, once again, the network-of-networks representation. In our setup, we assign a weight to each connection in \mathcal{P} such that links within physical nodes have weight 1 and links connecting two physical nodes have weight w , capturing that in real physical networks bonds between nodes are often qualitatively different than those within nodes. The weighted Laplacian matrix of \mathcal{P} occupying V sites is then $\mathbf{Q}_{\mathcal{P}} = \mathbf{D}_{\mathcal{P}} - \mathbf{A}_{\mathcal{P}}$, where $\mathbf{A}_{\mathcal{P}}$ is the $V \times V$ weighted adjacency matrix and $\mathbf{D}_{\mathcal{P}}$ is a diagonal matrix such that $[\mathbf{D}_{\mathcal{P}}]_{ss} = \sum_u [\mathbf{A}_{\mathcal{P}}]_{su}$ is the sum of the weights of the links adjacent to site s in \mathcal{P} . If we now set $w = 0$, the network-of-networks falls apart and each physical node becomes a separate connected component, resulting in a block-diagonal Laplacian $\mathbf{Q}_{\mathcal{P}}(0) = \text{diag}(\mathbf{Q}_{\mathcal{V}_1}, \mathbf{Q}_{\mathcal{V}_2}, \dots, \mathbf{Q}_{\mathcal{V}_N})$, where $\mathbf{Q}_{\mathcal{V}_i}$ is the Laplacian of the physical node \mathcal{V}_i . The Laplacian $\mathbf{Q}_{\mathcal{P}}(0)$ has N zero eigenvalues corresponding to the N blocks (i.e., the physical nodes), hence we can assign an eigenvector $\mathbf{u}_i(w = 0)$ to the i -th node such that $[\mathbf{u}_i(0)]_s = 1/\sqrt{v_i}$ if site s is within node i , otherwise $[\mathbf{u}_i(0)]_s = 0$, where $v_i = |\mathcal{V}_i|$ is the volume of node i . Since linear combinations of these vectors are also eigenvectors, we can write the zero eigenvectors of $\mathbf{Q}_{\mathcal{P}}$ as $\mathbf{u}(0) = \mathbf{M}\tilde{\mathbf{u}}$, where \mathbf{M} is the $N \times V$ membership matrix such that $[\mathbf{M}]_{si} = 1/\sqrt{v_i}$ if site s is part of node i , otherwise $[\mathbf{M}]_{si} = 0$, and $\tilde{\mathbf{u}}$ is any normalized N dimensional vector.

We can gain insights about the spectral properties of $\mathbf{Q}_{\mathcal{P}}$ by working in the weak coupling regime $w \ll 1$ and relying on perturbation theory. Following a treatment similar to the one adopted to study diffusion in multilayer networks [38–40], we consider w a small perturbation and write $\mathbf{Q}_{\mathcal{P}}(w) = \mathbf{Q}_{\mathcal{P}}(0) + w\mathbf{Q}'_{\mathcal{P}}$, where $\mathbf{Q}'_{\mathcal{P}}$ is the Laplacian matrix of the subnetwork of \mathcal{P} formed by the bonds

between physical nodes. The characteristic equation, up to first order in w , becomes then

$$\begin{aligned} (\mathbf{Q}_{\mathcal{P}}(0) + w\mathbf{Q}'_{\mathcal{P}})(\mathbf{u}(0) + w\mathbf{u}') &\approx \\ &\approx (\lambda(0) + w\lambda')(\mathbf{u}(0) + w\mathbf{u}'). \end{aligned} \quad (6)$$

Perturbations around $\lambda(0) = 0$ lead to N eigenvalues that are $\mathcal{O}(w)$, while the rest of the eigenvalues are constant in leading order (Fig. 3a). This means that on the $1/w$ timescale, diffusion-like dynamics on the physical network are captured by the N slow eigenmodes. We obtain these from Eq. (6) (see METHODS), yielding

$$\mathbf{V}^{-1/2}\mathbf{Q}_{\mathcal{G}}\mathbf{V}^{-1/2}\tilde{\mathbf{u}} = \lambda'\tilde{\mathbf{u}}, \quad (7)$$

where $\mathbf{Q}_{\mathcal{G}}$ is the $N \times N$ Laplacian matrix of the combinatorial network \mathcal{G} and \mathbf{V} is an $N \times N$ diagonal matrix such that its diagonal elements are $[\mathbf{V}]_{ii} = v_i$. We call the volume-normalized Laplacian the physical network Laplacian $\mathbf{Q}_{\text{phys}} = \mathbf{V}^{-1/2}\mathbf{Q}_{\mathcal{G}}\mathbf{V}^{-1/2}$.

Equation (7) is a key relation for understanding the dynamics on physical networks since it allows to characterize the dynamics on \mathcal{P} on the timescale $1/w$ in a coarse-grained way: after integrating out the fast modes corresponding to eigenvalues $\lambda(w) \gg w$, the state of each physical node \mathcal{V}_i is given by a single variable, while the coupling between the nodes is provided by the combinatorial network \mathcal{G} . However, the combinatorial Laplacian $\mathbf{Q}_{\mathcal{G}}$ is not sufficient to capture the dynamics, and we must normalize $\mathbf{Q}_{\mathcal{G}}$ by the volume of the nodes, as shown in Eq. (7). This means that physical networks with the same combinatorial network but different layout can have drastically different dynamical properties. For example, if nodes have approximately the same size, i.e., $v_i \approx V/N$, then the physical layout only affects the overall timescale, otherwise the Laplacian spectrum is determined by $\mathbf{Q}_{\mathcal{G}}$. If, however, node sizes are heterogeneously distributed, normalizing by volume will also have a heterogeneous effect on the eigenvalues.

Application to the physical network growth model. We showed above that physical networks generated by our network growth model are characterized by heterogeneous node-volume distribution and a proportionality between the degree and the volume of nodes (Fig. 2). To probe the effect of this emergent correlation, we shuffle the volume of the nodes of a LERW physical network to remove the correlation between network and physical structure. We then compare the spectrum of the volume-normalized Laplacian $\mathbf{Q}_{\text{phys}} = \mathbf{V}^{-1/2}\mathbf{Q}_{\mathcal{G}}\mathbf{V}^{-1/2}$ to its randomized version $\mathbf{Q}_{\text{phys}}^{\text{rand}} = \mathbf{V}_{\text{rand}}^{-1/2}\mathbf{Q}_{\mathcal{G}}\mathbf{V}_{\text{rand}}^{-1/2}$ and to the Laplacian spectrum of the combinatorial network $\mathbf{Q}_{\mathcal{G}}$. Figure 3b shows that the spectrum of $\mathbf{Q}_{\mathcal{G}}$ has a heavy tail characterized by the same γ exponent of Eq. (5), as expected for combinatorial networks with power law degree distributions [12]. Adding heterogeneous but uncorrelated node sizes does not influence the

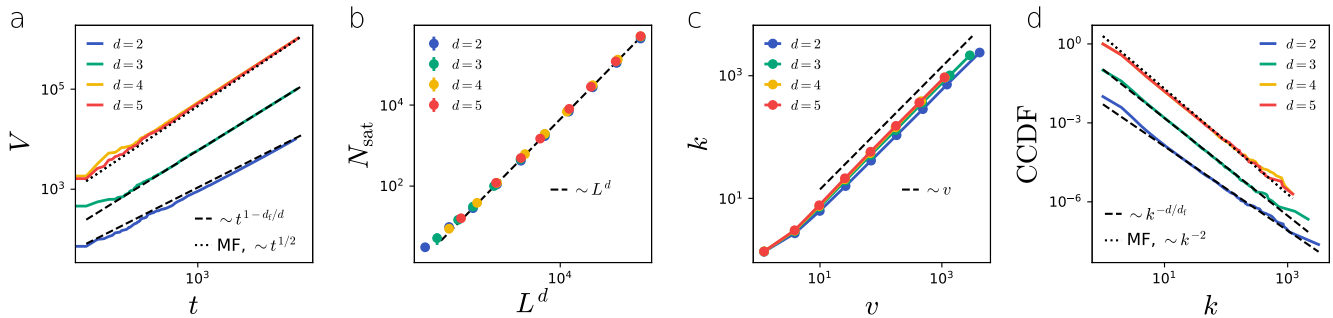


FIG. 2. **Evolution of LERW physical networks.** (a) The temporal evolution of the total volume V_i of physical networks, dashed lines represent the theoretical prediction Eq. (3). Networks built from LERWs in dimensions $d \geq 4$ fall into the mean-field regime. (b) The number of physical nodes in the saturated networks is proportional to the volume of the substrate $|\mathcal{S}|$ irrespective of d_f and d . (c) Node degree is proportional to node volume independently from d_f and d . (d) The complementary cumulative degree distribution function (CCDF) of the physical networks. Dashed lines indicate the predicted degree exponent $\gamma = 1 + d/d_f \leq 3$, while the dotted line corresponds to the mean-field behaviour $\gamma_{\text{MF}} = 3$. Plots (a), (c) and (d) represent measurements of single networks with initial condition $v_0 = L^{d_f}$ and $|\mathcal{S}| = 10^6$. In (b) markers are an average of 10 independent networks, error bars represent the standard error of the mean. Lines corresponding to different slopes are shifted to increase readability.

tail, while taking into account the degree-volume correlation of nodes removes the heavy tail and leads to a rapidly decaying spectrum. In power law networks, the eigenvector corresponding to the largest eigenvalue λ_N of \mathbf{Q}_G is typically concentrated on the node with the largest degree [41, 42]. In our model, the largest degree node also has the largest volume; therefore normalizing by node volume $\mathbf{V}^{-1/2} \mathbf{Q}_G \mathbf{V}^{-1/2}$ significantly lowers λ_N . Since node sizes are heterogeneously distributed, with high probability we associate volume ~ 1 to the highest degree node after randomization. Hence, the eigenvalue λ_N of \mathbf{Q}_G is largely unaffected by the randomized normalization (Fig. 3c). At the other end of the spectrum, controlling the long-time mixing of the dynamics, the eigenvector associated to the algebraic connectivity λ_2 typically spans the entire network. Figure 3d shows that taking node volumes into account slows the dynamics down; however, degree-volume correlations do not significantly affect λ_2 .

Note that positive degree-volume correlations, responsible for the suppression of the tail of the Laplacian spectrum, naturally arise in minimum volume physical realizations of combinatorial networks. Any combinatorial network \mathcal{G} has many possible physical realizations \mathcal{P} , a minimum volume realization is a \mathcal{P} that minimizes the total volume of the network. Consider node $i \in \mathcal{G}$ with degree k_i ; in any possible \mathcal{P} , the physical realization of node i must have volume at least proportional to k_i , otherwise it is unable to support k_i connections. Therefore, we expect positive degree-volume correlations in minimum volume physical layouts. This means that any physical network generation process that minimizes total volume – either explicitly or as an emergent property, like in our model – is characterized by positive degree-volume corre-

lations and hence that the spectrum of \mathbf{Q}_{phys} is similarly affected by physicality as in our model.

Real physical networks

We identified the degree-volume correlations and the shape of the Laplacian spectrum as important features of physical networks that can emerge even in the simplest models. To measure these properties, we do not need a detailed description of the layout of a physical system – we only need the combinatorial network and a list of the node volumes, allowing us to describe very large and complex physical networks. As a case study, we investigate a recently published data set providing the three-dimensional layout of more than 20,000 neurons of the brain of an adult fruit fly and the location of more than 13 million synapses connecting them (Fig. 4a) [15]. Although our simple growth model does not attempt to capture the myriad of complex mechanisms shaping brain development, we find that the fruit fly brain is characterized by similar emergent properties as the model networks. Figure 4b shows, for example, that the multiplicity-weighted node degree, i.e., the number of synapses a neuron has, can be approximated by a power law $\gamma_{\text{ff}} \approx 2.3$, albeit with an exponential cutoff [43, 44]. We also find a strong positive correlation between the weighted degree and the volume of the nodes (Fig. 4c).

To compare the spectrum of the combinatorial Laplacian \mathbf{Q}_G and the physical network Laplacian $\mathbf{Q}_{\text{phys}} = \mathbf{V}^{-1/2} \mathbf{Q}_G \mathbf{V}^{-1/2}$, we measure volume in units such that the mean node volume is unity, i.e., $\langle v \rangle = 1$ (see METHODS for further details). Calculating the leading eigenvalues of \mathbf{Q}_G and \mathbf{Q}_{phys} , we find that $\lambda_N^G / \lambda_N^{\text{phys}} \approx 32.7$,

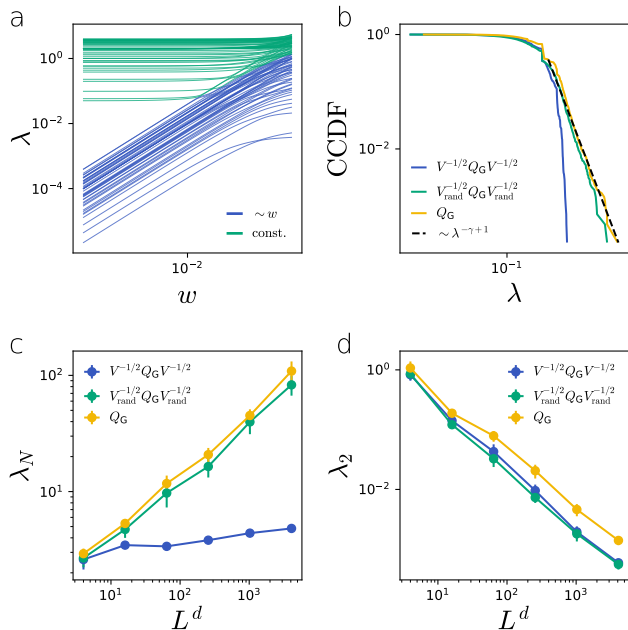


FIG. 3. **Laplacian of LERW physical networks.** (a) For decreasing weight w the eigenvalues of $\mathbf{Q}_{\mathcal{P}}$ separate into two groups: eigenvalues corresponding to the zero eigenmodes of $\mathbf{Q}_{\mathcal{P}}(w=0)$ decay as $\sim w$ (blue), while the rest converge to a constant value (teal). (b-d) Comparing the spectrum of the physical Laplacian $\mathbf{Q}_{\text{phys}} = \mathbf{V}^{-1/2} \mathbf{Q}_{\mathcal{G}} \mathbf{V}^{-1/2}$, the randomized Laplacian $\mathbf{Q}_{\text{phys}}^{\text{rand}} = \mathbf{V}_{\text{rand}}^{-1/2} \mathbf{Q}_{\mathcal{G}} \mathbf{V}_{\text{rand}}^{-1/2}$, and the Laplacian of the combinatorial network $\mathbf{Q}_{\mathcal{G}}$. (b,c) The heterogeneous node volume distribution and the correlation between node degree and volume significantly reduce the largest eigenvalues of the spectra. (d) Heterogeneous node volumes alone explain the reduction of the algebraic connectivity λ_2 . Eigenvalues are calculated for $d=2$ and $L=10$ in (a) and $L=100$ in (b). In (c) and (d) markers are an average of 10 independent networks, error bars represent the standard error of the mean.

indicating that degree-volume correlations greatly suppress the modes of the dynamics that spread the fastest, similarly to model networks. This is further supported by Fig. 4d, showing again that physicality suppresses the tail of the spectrum.

To further probe the role of degree-volume correlations, we calculate the leading eigenvectors $\tilde{\mathbf{u}}_N$ of $\mathbf{Q}_{\mathcal{G}}$ and \mathbf{Q}_{phys} . Figures 4e,g show that, as expected for heterogeneous combinatorial networks, $\tilde{\mathbf{u}}_N^{\mathcal{G}}$ is concentrated on the largest hub $i_{\mathcal{G}}$ in the network, and the weight of the eigenvector decays exponentially as the geodesic distance from $i_{\mathcal{G}}$ in \mathcal{G} . This means that, without taking physicality into account, the largest degree node is also the earliest spreader of diffusive dynamics. For the physical Laplacian \mathbf{Q}_{phys} we find a different picture: $\tilde{\mathbf{u}}_N^{\text{phys}}$ is again concentrated on a single node i_{phys} ; this node, however, is not the largest hub. The leading eigenvector instead is centered on a node that balances high degree and low volume: node i_{phys} is the 159th largest de-

gree node and is at the top 15 percentile of the volume distribution. In fact, node i_{phys} is the node that maximizes the degree-volume ratio, i.e., $i_{\text{phys}} = \text{argmax}_i k_i/v_i$. This means that degree-volume correlations not only slow down spreading dynamics in physical networks, but also change the identity of the early spreaders.

Here we chose to focus on the fruit fly brain network as it represents one of the largest and most detailed maps of physical networks available; however, our framework is not specific to neural networks. In the Sec. S2 of the Supplementary Information, we analyze four additional real systems: a network describing the cavities of a porous material, a neural network of a nematode, a river network and a vascular network. In each case, we find positive degree-volume correlations and that these correlations suppress the tail of the Laplacian spectra. The fact that the physical and network properties of nodes become intertwined in such a diverse set of real networks, and also in the simplest models, indicates a general mechanism behind the emergence of degree-volume correlations that does not depend on the details of the individual networks.

DISCUSSION

Physical networks are complex networks that have a complex three-dimensional layout. The network-of-networks framework naturally lends itself to represent these systems: representing nodes as physically embedded networks allows us to capture arbitrary node shapes and complex wiring. Here, we relied on the network-of-networks framework to characterize both model and real physical networks. We identified correlations between node degree and volume as a prevalent feature of physical networks: We analytically showed that degree-volume correlations emerge in a minimal network growth model, in fact, we provided arguments that such correlations naturally arise through any growth process that minimizes network volume. We also showed that positive degree-volume correlations are generally present in real systems. These correlations have important consequences on dynamics unfolding on physical networks: the tail of the physical Laplacian spectrum is suppressed by the large volume of hubs. More broadly, these results vividly demonstrate that traditional methods of network science focusing on combinatorial networks cannot fully describe physical networks and that their three-dimensional layout must be accounted for.

Our work opens new avenues for physical network research in several ways. First, by establishing the connection between physical networks and network-of-networks, we allow future work to leverage the rich literature of multi-layer networks to characterize physical systems [10, 11]. For example, multi-layer centrality measures can be used to quantify the importance of physical

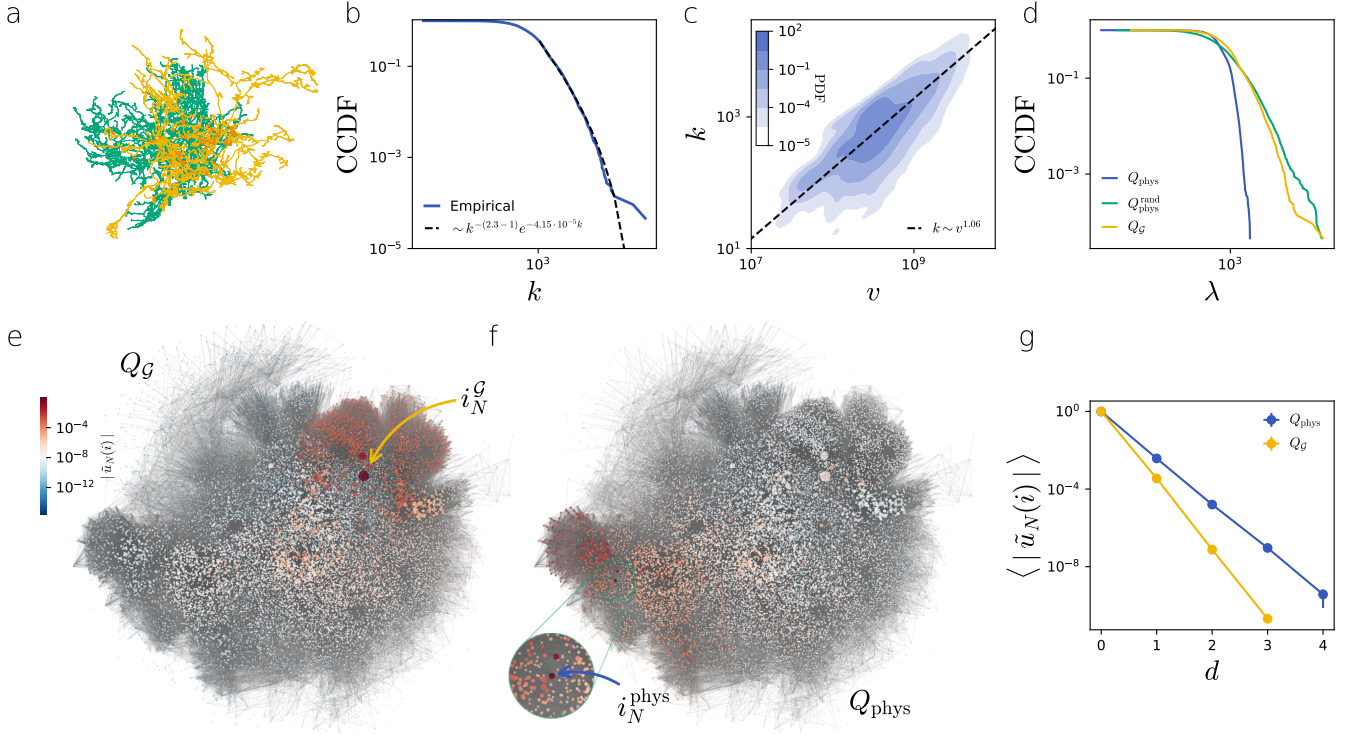


FIG. 4. **Fruit fly brain network.** (a) The neurons have complex three-dimensional shapes. Two intertwined neurons (teal and yellow) are connected by synapses (red circles). (b) The tail of the weighted degree distribution can be approximated with the power law with $\gamma_{\text{fit}} \approx 2.3$ with an exponential cutoff. (c) Similar to the network growth model, the volume of the nodes v is strongly correlated with their degree k . The markers indicate binned degree-volume averages, where the data points are binned based on node volume. The shading represents a kernel density estimate of the joint v - k distribution, the dashed line indicates the least squares fit of the power law scaling. (d) The effect of the node degree-volume correlation on the Laplacian spectrum in the brain network is analog to the effect of correlations in the network growth model. The spectra of \mathbf{Q}_{phys} and $\mathbf{Q}_{\text{phys}}^{\text{rand}}$ are shifted to the right to allow direct comparison of the tails of the distributions. (e-f) A visualization of the leading eigenvectors $\tilde{\mathbf{u}}_N$ of the combinatorial and physical Laplacians. The color of each node i corresponds to $|\tilde{u}_N(i)|$, the weight of the leading eigenvector at node i , and the size of the nodes is a linear function of their degree. (e) The eigenvector $\tilde{\mathbf{u}}_N^{\mathcal{G}}$ is concentrated on the node with the highest degree $i_{\mathcal{G}}$. (f) Due to degree-volume correlations, the $\tilde{\mathbf{u}}_N^{\text{phys}}$ is concentrated on node i_{phys} , which has the maximum degree-volume ratio in the network. (g) The weight of the leading eigenvectors $|\tilde{u}_N^{\mathcal{G}}(i)|$ and $|\tilde{u}_N^{\text{phys}}(i)|$ decays exponentially as a function of the geodesic distance from $i_{\mathcal{G}}$ and i_{phys} , respectively. Error bars indicate the standard error of the mean and are typically smaller than the marker size. Node locations in (e) and (f) are generated based on \mathcal{G} , and do not correspond to the actual physical locations.

nodes [45–47]. Second, previous work on physical networks rely on methods that require full description of their spatial layout; and therefore are often limited to systems of a few hundred nodes [1–3]. In contrast, the quantities we studied can be measured relying on the combinatorial network and a list of node volumes, allowing the characterization of large-scale physical networks without the need of the full three-dimensional layout. For example, we can tune the volume of the nodes to systematically study how physical layout affects the Laplacian spectrum. Finally, the simple growth model and its analytical description can serve as the starting point of exploration of additional growth mechanisms that characterize

neural networks and other physical networks. For example, future work may study branched nodes, long-range interactions that guide the growth of physical nodes, or the expansion of available space by modeling the evolution of the underlying substrate.

METHODS

Loop-erased random walks. In our network growth model, we can generate physical nodes with any stochastic or deterministic process that produces a growing fractal embedded in \mathbb{Z}^d . Standard self-avoiding walks are traditionally used to model polymers obeying volume exclusion, and therefore represent a natural choice to model node growth [17]. However, the naïve kinetic version of the self-avoiding walk traps itself in two and three dimensions at finite length [21], making it a poor candidate to construct large physical networks. Instead, we focus on loop-erased random walks (LERW): a LERW evolves as a simple random walk, except when it intersects itself, we delete the loop that it created and continue the walk [20]. This guarantees that the final physical node does not intersect itself and that the walk never gets trapped. Alternatively, the LERW can be defined as special case of Laplacian-random walks, where transition probabilities are defined by a harmonic function [48, 49]. This alternative construction does not require deleting loops, hence is more realistic as a growth model. The LERW has attractive mathematical properties making it amenable to analytical treatment. For example, Wilson’s algorithm uses iterative LERWs to construct a uniform spanning tree (UST) of any graph [24]. In fact, the physical network our algorithm constructs is a UST of the \mathcal{S} substrate together with a partition identifying the nodes. Future work may exploit this connection between USTs and LERW physical networks, together with known results in dimensions $d = 2$ and $d > 4$ [22, 50], to rigorously prove some of the results presented here.

Perturbation of the physical Laplacian. To obtain the slow eigenmodes, we match the first order terms of Eq. (6) and substitute $\mathbf{u}(0) = \mathbf{M}\tilde{\mathbf{u}}$, so that

$$\mathbf{Q}_{\mathcal{P}}(0)\mathbf{u}' + \mathbf{Q}'_{\mathcal{P}}\mathbf{M}\tilde{\mathbf{u}} = \lambda'\mathbf{M}\tilde{\mathbf{u}}. \quad (8)$$

Multiplying from the left by the transpose of the membership matrix \mathbf{M} we get

$$\mathbf{M}^T\mathbf{Q}_{\mathcal{P}}(0)\mathbf{u}' + \mathbf{M}^T\mathbf{Q}'_{\mathcal{P}}\mathbf{M}\tilde{\mathbf{u}} = \lambda'\mathbf{M}^T\mathbf{M}\tilde{\mathbf{u}}. \quad (9)$$

The i th row of \mathbf{M}^T is the trivial eigenvector $\mathbf{u}_i(w=0)$ corresponding to physical node i ; therefore $\mathbf{M}^T\mathbf{Q}_{\mathcal{P}}(0)$ is all zeros and $\mathbf{M}^T\mathbf{M}$ is the $N \times N$ identity matrix, leading to Eq. (7) in the text.

The fruit fly connectome. We study the Hemibrain data set which describes a portion of the central brain of the fruit fly, *Drosophila melanogaster* [15]. The physical layout of the connectome is provided by the detailed three-dimensional shape of each neuron and the location of the synapses between them. The corresponding combinatorial network contains 21,662 nodes representing neurons and 13,603,750 links representing synapses. Synaptic partners are connected through approximately 5 synapses on average, and the maximum number of

synapses between two neurons is 6039. In our calculations, we treat the combinatorial network as a weighted and undirected network, where the weight of link (i, j) is equal to the number of synapses between neuron i and j . Note that we only require the combinatorial network and the volume of each node for our calculations; therefore the detailed physical layout of the connectome is in fact not needed.

Note that the Hemibrain data set covers a large portion of, but not the entire, fruit fly brain. Since degree and volume are local properties of the nodes, we expect that the results presented here would not change significantly if the entire connectome were to be considered.

Degree distribution. We find that the weighted degree distribution has a heavy tail, which can be approximated by a power law with $\gamma_{\text{ff}} \approx 2.3$ for degrees ≥ 1058 with an exponential cutoff; the power law fit, however, cannot be distinguished from a lognormal fit on the same range [43, 44].

Laplacian spectrum. Comparing the spectrum of the combinatorial Laplacian $\mathbf{Q}_{\mathcal{G}}$ and the volume-normalized Laplacian $\mathbf{Q}_{\text{phys}} = \mathbf{V}^{-1/2}\mathbf{Q}_{\mathcal{G}}\mathbf{V}^{-1/2}$ carries a level of ambiguity: $\mathbf{Q}_{\mathcal{G}}$ does not depend on the node volumes, while changing the unit of volume multiplies the spectrum of \mathbf{Q}_{phys} by a constant. To meaningfully compare the two spectra, (i) we think of $\mathbf{Q}_{\mathcal{G}}$ as a physical Laplacian where all nodes have unit volume, and (ii) we set the mean node volume in \mathbf{Q}_{phys} to unity, i.e., $\langle v \rangle = 1$. With this choice of units, any difference in the eigenvalues is due to the heterogeneous distribution of node volumes in the physical network and not to a global shift caused by the choice of units.

DATA AVAILABILITY

Data to reproduce the figures is available at https://github.com/posfaim/physnets_as_net-o-nets.

CODE AVAILABILITY

Code to generate random networks and reproduce the figures is available at https://github.com/posfaim/physnets_as_net-o-nets [51].

-
- [1] N. Dehmamy, S. Milanlouei, and A.-L. Barabási. A structural transition in physical networks. *Nature*, 563(7733):676–680, 2018.
 - [2] Y. Liu, N. Dehmamy, and A.-L. Barabási. Isotopy and energy of physical networks. *Nature Physics*, 17(2):216–222, 2021.

- [3] Márton Pósfai, Balázs Szegedy, Iva Bačić, Luka Blagojević, Miklós Abért, János Kertész, László Lovász, and Albert-László Barabási. Impact of physicality on network structure. *Nature Physics*, 20:142–149, 2024.
- [4] E. Bullmore and O. Sporns. Complex brain networks: graph theoretical analysis of structural and functional systems. *Nature Reviews Neuroscience*, 10(3):186–198, 2009.
- [5] M. P. Viana, A. I. Brown, I. A. Mueller, C. Goul, E. F. Koslover, and S. M. Rafelski. Mitochondrial fission and fusion dynamics generate efficient, robust, and evenly distributed network topologies in budding yeast cells. *Cell systems*, 10(3):287–297, 2020.
- [6] D. A. Fletcher and R. D. Mullins. Cell mechanics and the cytoskeleton. *Nature*, 463(7280):485–492, 2010.
- [7] Catalin R Picu. *Network Materials: Structure and Properties*. Cambridge University Press, Cambridge, 2022.
- [8] S. W Simard, D. A. Perry, M. D. Jones, D. D. Myrold, D. M. Durall, and R. Molina. Net transfer of carbon between ectomycorrhizal tree species in the field. *Nature*, 388(6642):579–582, 1997.
- [9] B. S. Steidinger, T. W Crowther, J. Liang, M. E. Van Nuland, G. D. A. Werner, P. B. Reich, G.-J. Nabuurs, S. de Miguel, M. Zhou, N. Picard, et al. Climatic controls of decomposition drive the global biogeography of forest-tree symbioses. *Nature*, 569(7756):404–408, 2019.
- [10] M. De Domenico, A. Solé-Ribalta, E. Cozzo, M. Kivelä, Y. Moreno, M. A. Porter, S. Gómez, and A. Arenas. Mathematical formulation of multilayer networks. *Physical Review X*, 3(4):041022, 2013.
- [11] G. Bianconi. *Multilayer networks: structure and function*. Oxford University Press, Oxford, 2018.
- [12] P. Van Mieghem. *Graph spectra for complex networks*. Cambridge University Press, Cambridge, 2010.
- [13] C. Castellano and R. Pastor-Satorras. Relating topological determinants of complex networks to their spectral properties: Structural and dynamical effects. *Physical Review X*, 7(4):041024, 2017.
- [14] P. Villegas, T. Gili, G. Caldarelli, and A. Gabrielli. Laplacian renormalization group for heterogeneous networks. *Nature Physics*, pages 1–6, 2023.
- [15] L. K. et al. Scheffer. A connectome and analysis of the adult drosophila central brain. *Elife*, 9:e57443, 2020.
- [16] R. Tamassia, editor. *Handbook of graph drawing and visualization*. CRC Press, Boca Raton, FL, 2013.
- [17] T. Vicsek. *Fractal growth phenomena*. World Scientific, Singapore, 1992.
- [18] A. Bunde and S. Havlin, editors. *Fractals and disordered systems*. Springer Berlin, Heidelberg, 2012.
- [19] P.-G. de Gennes. Exponents for the excluded volume problem as derived by the wilson method. *Phys. Lett. A*, 38(5):339–340, 1972.
- [20] G. F. Lawler. A self-avoiding random walk. *Duke Math. J.*, 47(3):655–693, 1980.
- [21] L. Pietronero. Survival probability for kinetic self-avoiding walks. *Phys. Rev. Lett.*, 55(19):2025, 1985.
- [22] O. Schramm. Scaling limits of loop-erased random walks and uniform spanning trees. *Israel Journal of Mathematics*, 118(1):221–288, 2000.
- [23] L. Niemeyer, L. Pietronero, and H. J. Wiesmann. Fractal dimension of dielectric breakdown. *Phys. Rev. Lett.*, 52(12):1033, 1984.
- [24] D. B. Wilson. Generating random spanning trees more quickly than the cover time. In *Proceed. of the 28th ACM Theory of computing*, pages 296–303, 1996.
- [25] Gregory F Lawler, Oded Schramm, and Wendelin Werner. Conformal invariance of planar loop-erased random walks and uniform spanning trees. *Annals of probability*, 32(1):939–995, 2004.
- [26] K. Wiese and A. A. Fedorenko. Field theories for loop-erased random walks. *Nuclear Physics B*, 946:114696, 2019.
- [27] H. Agrawal and D. Dhar. Distribution of sizes of erased loops of loop-erased random walks in two and three dimensions. *Phys. Rev. E*, 63(5):056115, 2001.
- [28] P. Grassberger. Scaling of loop-erased walks in 2 to 4 dimensions. *Journal of statistical physics*, 136:399–404, 2009.
- [29] D. B. Wilson. Dimension of the loop-erased random walk in three dimensions. *Phys. Rev. E*, 82(6):062102, 2010.
- [30] A. Barrat, M. Barthelemy, and A. Vespignani. *Dynamical processes on complex networks*. Cambridge University Press, Cambridge, 2008.
- [31] N. Masuda, M. A. Porter, and R. Lambiotte. Random walks and diffusion on networks. *Phys. Rep.*, 716:1–58, 2017.
- [32] M. De Domenico and J. Biamonte. Spectral entropies as information-theoretic tools for complex network comparison. *Phys. Rev. X*, 6(4):041062, 2016.
- [33] A. Arenas, A. Diaz-Guilera, J. Kurths, Y. Moreno, and C. Zhou. Synchronization in complex networks. *Phys. Rep.*, 469(3):93–153, 2008.
- [34] Marian Boguna, Ivan Bonamassa, Manlio De Domenico, Shlomo Havlin, Dmitri Krioukov, and M Ángeles Serrano. Network geometry. *Nature Reviews Physics*, 3(2):114–135, 2021.
- [35] Arsham Ghavasieh, Massimo Stella, Jacob Biamonte, and Manlio De Domenico. Unraveling the effects of multiscale network entanglement on empirical systems. *Communications Physics*, 4(1):129, 2021.
- [36] P. Villegas, A. Gabrielli, F. Santucci, G. Caldarelli, and T. Gili. Laplacian paths in complex networks: Information core emerges from entropic transitions. *Phys. Rev. Res.*, 4(3):033196, 2022.
- [37] Arsham Ghavasieh and Manlio De Domenico. Generalized network density matrices for analysis of multiscale functional diversity. *Physical Review E*, 107(4):044304, 2023.
- [38] S. Gomez, A. Diaz-Guilera, J. Gomez-Gardenes, C. J. Perez-Vicente, Y. Moreno, and A. Arenas. Diffusion dynamics on multiplex networks. *Phys. Rev. Lett.*, 110(2):028701, 2013.
- [39] A. Solé-Ribalta, M. De Domenico, N. E. Kouvaris, A. Diaz-Guilera, S Gomez, and A. Arenas. Spectral properties of the laplacian of multiplex networks. *Physical Review E*, 88(3):032807, 2013.
- [40] F. Radicchi and A. Arenas. Abrupt transition in the structural formation of interconnected networks. *Nature Physics*, 9(11):717–720, 2013.
- [41] R. Pastor-Satorras and C. Castellano. Distinct types of eigenvector localization in networks. *Sci. Rep.*, 6(1):18847, 2016.
- [42] S. Hata and H. Nakao. Localization of laplacian eigenvectors on random networks. *Sci. Rep.*, 7(1):1–11, 2017.
- [43] Aaron Clauset, Cosma Rohilla Shalizi, and Mark EJ Newman. Power-law distributions in empirical data. *SIAM Review*, 51(4):661–703, 2009.

- [44] Jeff Alstott, Ed Bullmore, and Dietmar Plenz. powerlaw: a python package for analysis of heavy-tailed distributions. *PLoS one*, 9(1):e85777, 2014.
- [45] Arda Halu, Raúl J Mondragón, Pietro Panzarasa, and Ginestra Bianconi. Multiplex pagerank. *PLoS one*, 8(10):e78293, 2013.
- [46] Albert Solé-Ribalta, Manlio De Domenico, Sergio Gómez, and Alex Arenas. Centrality rankings in multiplex networks. In *Proceedings of the 2014 ACM conference on Web science*, pages 149–155, 2014.
- [47] Jacopo Iacovacci, Christoph Rahmede, Alex Arenas, and Ginestra Bianconi. Functional multiplex pagerank. *Europhysics Letters*, 116(2):28004, 2016.
- [48] J. W. Lyklema, C. Evertsz, and L. Pietronero. The laplacian random walk. *EPL (Europhysics Letters)*, 2(2):77, 1986.
- [49] G. F. Lawler. Loop-erased self-avoiding random walk and the laplacian random walk. *Journal of Physics A: Mathematical and General*, 20(13):4565, 1987.
- [50] S. Bhupatiraju, J. Hanson, and A. A. Járαι. Inequalities for critical exponents in d-dimensional sandpiles. 2017.
- [51] Márton Pósfai. posfaim/physnets_as_net-o-nets: Physical networks as network-of-networks. <https://doi.org/10.5281/zenodo.11140782>, 2024.

10.5281/zenodo.11140782, 2024.

ACKNOWLEDGMENTS

IB, MP and ÁT were funded by ERC grant No. 810115-DYNASNET. ÁT and SÖS acknowledge partial support from the Icelandic Research Fund, grant No. 239736-051. GP was funded by the ERC Consolidator Grant No. 772466-NOISE.

AUTHOR CONTRIBUTIONS STATEMENT

MP developed and performed the numerical simulations. MP and IB performed the data analysis. GP, ÁT, SÖS, IB and MP contributed to the analytical results and the conceptual design of the study. MP was the lead writer of the manuscript.

COMPETING INTERESTS STATEMENT

The authors declare no competing interests.

Supplementary Information – Physical networks as network-of-networks

Gábor Pete,^{1,2,*} Ádám Timár,^{1,3} Sigurdur Örn Stefánsson,³

Ivan Bonamassa,⁴ and Márton Pósfai^{4,†}

¹*Alfréd Rényi Institute of Mathematics, Budapest, Hungary*

²*Budapest University of Technology and Economics, Budapest, Hungary*

³*University of Iceland, Reykjavík, Iceland*

⁴*Department of Network and Data Science,
Central European University, Vienna, Austria*

CONTENTS

S1. Physical node growth algorithms	2
S2. Empirical physical networks	17
Supplementary references	21

* gabor.pete@renyi.hu

† posfaim@ceu.edu

S1. PHYSICAL NODE GROWTH ALGORITHMS

Relying on the network-of-networks representation of physical networks, we introduced a simple model of physical network evolution in the main text. In the model, physical nodes are added sequentially and grow following a random trajectory until they connect to the existing network. The analytical description of the model imposes mild restrictions on the random trajectory that grows the physical nodes: the trajectory must be described by a fractal dimension $d_f \in [1, d]$ (where d is the embedding dimension) and the random trajectories need to have the property that if the boxes around two random walk pieces intersect, then with uniformly positive probability the pieces also intersect. This latter condition requires a level of isotropy, at least on average. For a simple counterexample, consider nodes embedded in a two dimensional square lattice always growing along the horizontal axis; in this case two nodes can run parallel to each other with overlapping bounding boxes without intersecting, and the resulting network will be a collection of disconnected chains.

The analytical description of the model presented in the main text predicts that independent of the details of the physical node trajectories, the degree distribution of the emergent physical network has a power law tail; however the exact value of the degree exponent γ does depend on d_f . Specifically, we make the following predictions:

- The total volume of the network grows as

$$V_t \sim L^d \left(\frac{t}{L^d} \right)^{1-d_f/d}, \quad (\text{S1})$$

where L is the linear dimension of the embedding d dimensional square lattice.

- For large nodes, the degree of the physical nodes is proportional their volume

$$k_t(N) = 1 + \frac{v_t}{L^d} \sum_{s=t+1}^N v_s^{d/d_f-1} \sim v_t \cdot \left(\frac{N}{L^d} \right)^{\frac{d}{d_f}}. \quad (\text{S2})$$

- The tail of the degree distribution is characterized by a power law $P(k) \sim k^{-(\gamma-1)}$ with exponent

$$\gamma = 1 + \frac{d}{d_f}, \quad (\text{S3})$$

for $2d_f > d$, for $2d_f \leq d$ we are in the meanfield regime with $\gamma_{\text{MF}} = 3$.

In the remainder of this section we compare the above predictions to numerical simulations using a wide range of random node trajectories, in addition to loop-erased random walk node trajectories studied in the main text.

S1.1. Meanfield node growth: random point cloud

In the meanfield regime ($2d_f < d$) the fractal dimension d_f of the physical nodes is so small that even if the boxes containing two nodes \mathcal{V}_i and \mathcal{V}_j overlap, nodes i and j avoid each other with high probability. In this regime the network evolution follows the characteristics of the network evolution in infinite dimensions $d = \infty$, i.e., the substrate \mathcal{S} is a complete graph. To simulate meanfield dynamics, we can equivalently grow physical nodes by random jumps:

- We embed the growing network in a finite d -dimensional lattice.
- Each physical node \mathcal{V}_t is grown by adding a uniformly random lattice site to \mathcal{V}_t .

Note that the lattice sites that we sequentially add to \mathcal{V}_t are not necessarily adjacent, and \mathcal{V}_t is typically not a connected sub-graph of \mathcal{S} .

Figure S1 shows the physical layout \mathcal{P} and the combinatorial network \mathcal{G} of an example network generated using random jump nodes. Figure S2 compares the analytical predictions to simulations, finding excellent agreement.

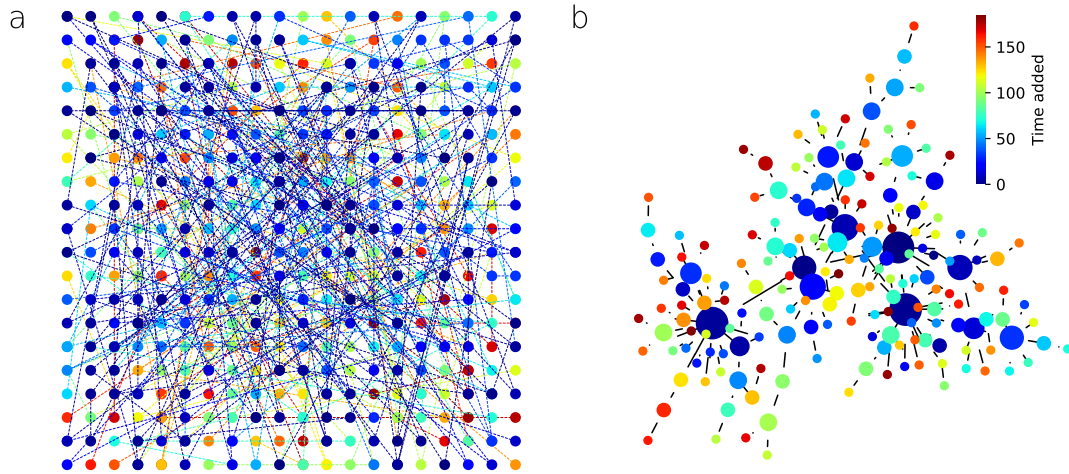


FIG. S1. **Example network generated with random jump nodes.** (a) The physical layout \mathcal{P} of a saturated network embedded in a 20×20 square lattice with periodic boundary conditions. The color of physical nodes indicate the time they were added. Sequential lattice sites in a physical node trajectory \mathcal{V}_t (connected by dashed lines) are typically non-adjacent. (b) The corresponding combinatorial network \mathcal{G} . Node sizes are a linear function of the logarithm of their degrees.

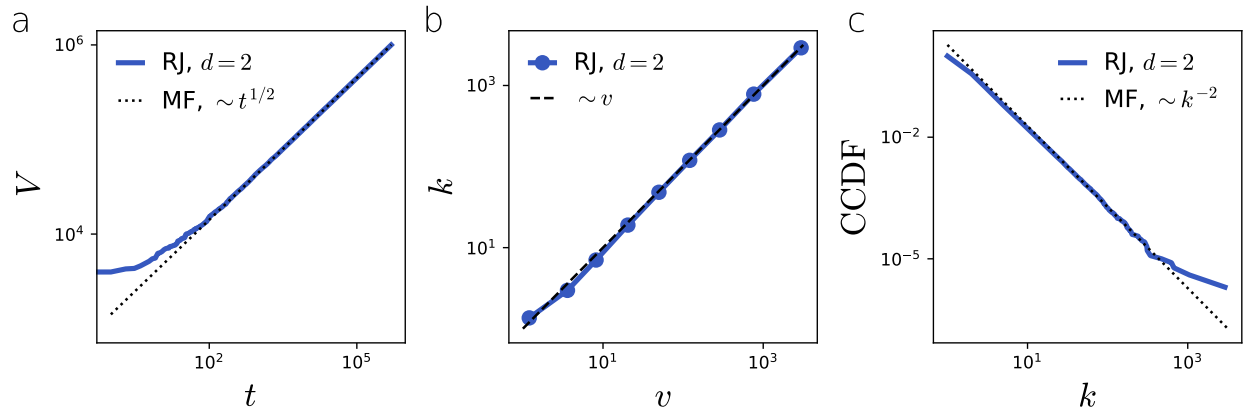


FIG. S2. **Random jump networks.** (a) Evolution of the total volume of the network V_t . (b) Correlations between node volume v and node degree degree k . (c) Complementary cumulative distribution of the node degree. (a-c) We compare the predictions of Eqs. (S1),(S2) and (S3) to numerical simulations, finding near perfect agreement. The lines indicate results for a single saturated network embedded on d -dimensional square lattice with periodic boundaries and side length L , where L is chosen such that $L^d \approx 10^6$.

S1.2. Simple random walk

We also generate physical nodes using trajectories of simple random walks (SRW). In this case, a physical node \mathcal{V}_i is allowed to intersect itself and halts its growth once it hits another \mathcal{V}_j ($i \neq j$). In other words, volume exclusion is only imposed between the trajectories of distinct nodes, i.e., $\mathcal{V}_i \cap \mathcal{V}_j$ still holds for $i \neq j$. The fractal dimension of SRWs is $d_f = 2$ for embedding dimensions $d \leq 2$, meaning that for $d \leq 4$ we are in the meanfield regime. Embedding dimension $d = 2$ also represents a special case $d = d_f$, for which Eq. (S1) predicts that the exponent of the total volume growth is $1 - d_f/d = 0$, and we expect that other effects not captured by the theory to become relevant. For example, since each new physical node starts from an unoccupied site, the minimum node volume in simulations is one, i.e., $|\mathcal{V}_i| \leq 1$, which becomes relevant if the predicted node volume falls below unity. Figure S3 shows the physical layout \mathcal{P} and the combinatorial network \mathcal{G} of an example network generated using SRWs. Figure S4 compares the analytical predictions to simulations, finding excellent agreement.

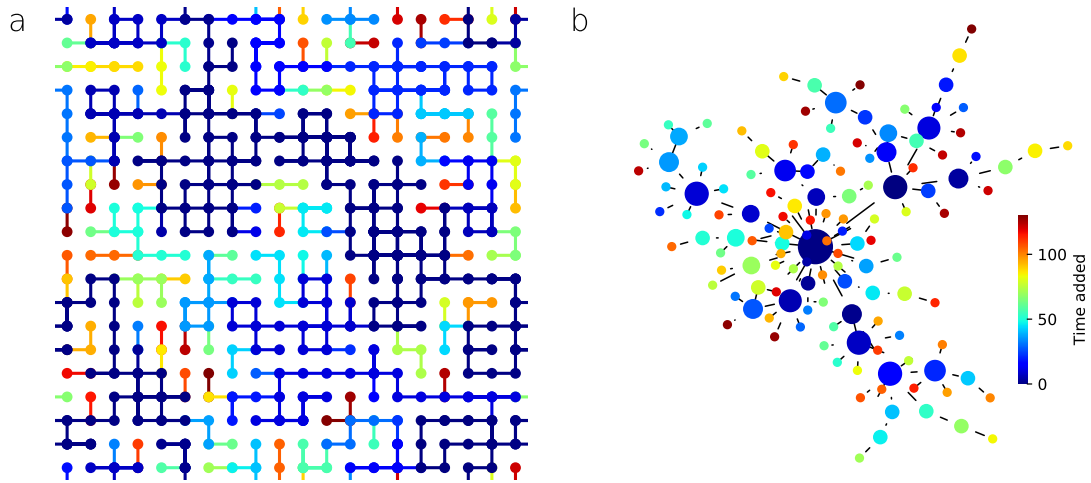


FIG. S3. **Example network generated with SRWs.** (a) The physical layout \mathcal{P} of a saturated network embedded in a 20×20 square lattice with periodic boundary conditions. The color of physical nodes indicate the time they were added. A SRW trajectory may intersect itself. (b) The corresponding combinatorial network \mathcal{G} . Node sizes are a linear function of the logarithm of their degrees.

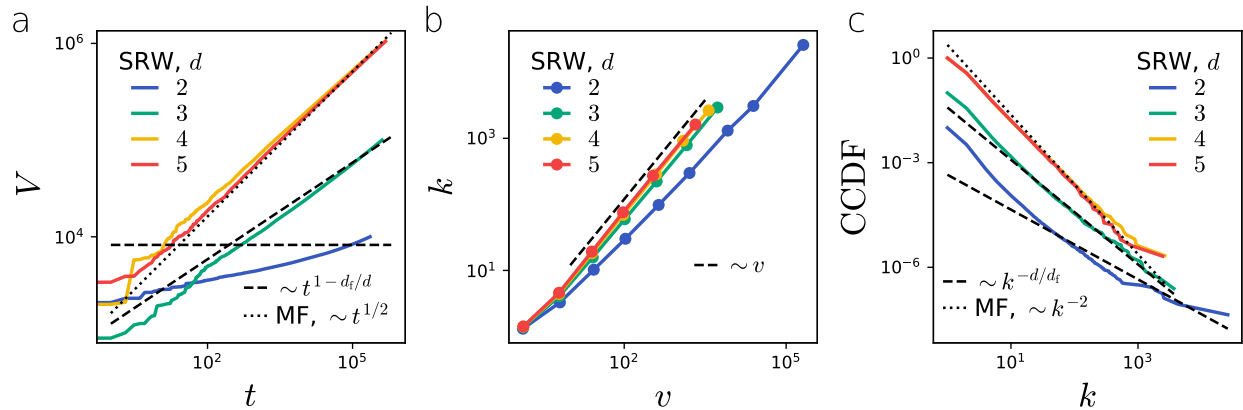


FIG. S4. **SRW networks.** (a) Evolution of the total volume of the network V_t . (b) Correlations between node volume v and node degree degree k . (c) Complementary cumulative distribution of the node degree. (a-c) We compare the predictions of Eqs. (S1),(S2) and (S3) to numerical simulations, finding excellent agreement. The lines indicate results for a single saturated network embedded on d -dimensional square lattice with periodic boundaries and side length L , where L is chosen such that $L^d \approx 10^6$.

S1.3. Kinetic self-avoiding random walk

We also test our predictions against networks grown from kinetic self-avoiding random walk (KSAW) trajectories. Self-avoiding random walks were introduced to model polymer chains, and are most often studied in an equilibrium setting, i.e., in an equilibrium ensemble all self-avoiding trajectories of a given length have the same weight [1]. Here, we grow physical nodes using the kinetic version, also called genuine self-avoiding walks: a walker starts from a random lattice site and always moves to a uniformly chosen adjacent site that it has not visited before [2]. Such random walks seem as a natural choice for our network model; however, the KSAW traps itself in two and three dimensions after a finite number of steps. In large lattices ($L \rightarrow \infty$), the expected maximum volume of KSAW trajectories is approximately $v_2^{\max} \approx 71$ in two dimensions and $v_3^{\max} \approx 4000$ in three dimensions S5 [3]. This means that it becomes impossible to grow physical networks using our original model for $L \ll v^{\max}$ embedding lattices, as a result we only simulate networks for $d \leq 3$ on lattices with $L^d \approx 10^6$ sites.

In three dimensions the fractal dimension of SAWs is $d_f \approx 1.7$, above three dimensions the probability of self-intersection asymptotically becomes zero and SAWs are characterized by the fractal dimension of SRWs, i.e., $d_f = 2$ for $d \leq 4$ [4]. This means that KSAW networks are in the meanfield regime for dimensions $d > 3$. Figure S6 shows the physical layout \mathcal{P} and the combinatorial network \mathcal{G} of an example network generated using KSAWs. Figure S7 compares the analytical predictions to simulations, finding excellent agreement.

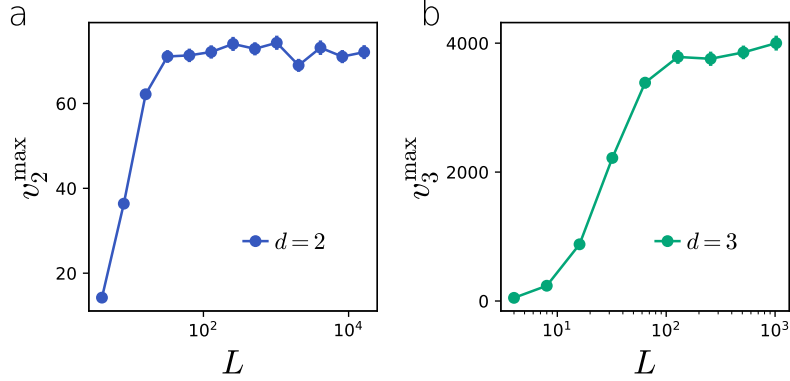


FIG. S5. **Self-trapping of KSAW trajectories.** (a) Expected maximum volume of a KSAW trajectory for embedding dimension $d = 2$ and (b) embedding dimension $d = 3$. (a-b) We grow KSAW trajectories in isolation until they get trapped, i.e., all sites adjacent to the walker have been visited before, and we measure their final volume v^{\max} as a function of lattice size L . On finite lattices, all walkers eventually get trapped, the fact that v^{\max} plateaus and becomes independent of L indicates that KSAWs trap themselves in the $L \rightarrow \infty$ limit for $d = 2$ and $d = 3$. Markers represent an average of 1000 independent runs and the errorbars provide the standard error of the mean.

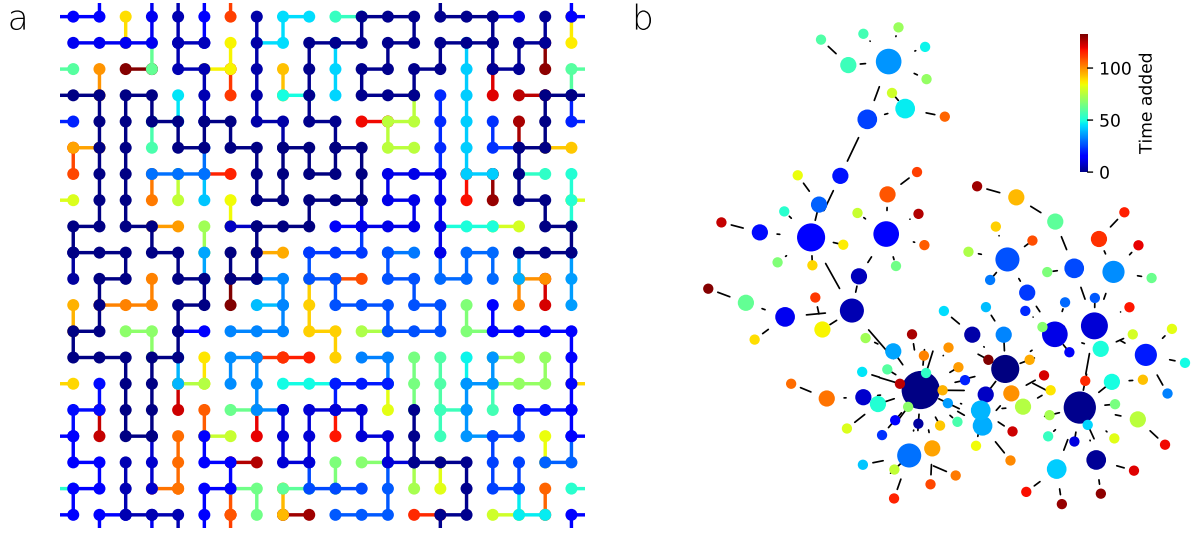


FIG. S6. **Example network generated with KSAWs.** (a) The physical layout \mathcal{P} of a saturated network embedded in a 20×20 square lattice with periodic boundary conditions. The color of physical nodes indicate the time they were added. A KSAW trajectory traps itself after $v_2^{\max} \approx 71$ steps in 2 dimensions; therefore, we would not be able to generate KSAW networks for $L \ll 71$ for $d = 2$. In this simulation, we restart the growth of nodes that got trapped. (b) The corresponding combinatorial network \mathcal{G} . Node sizes are a linear function of the logarithm of their degrees.

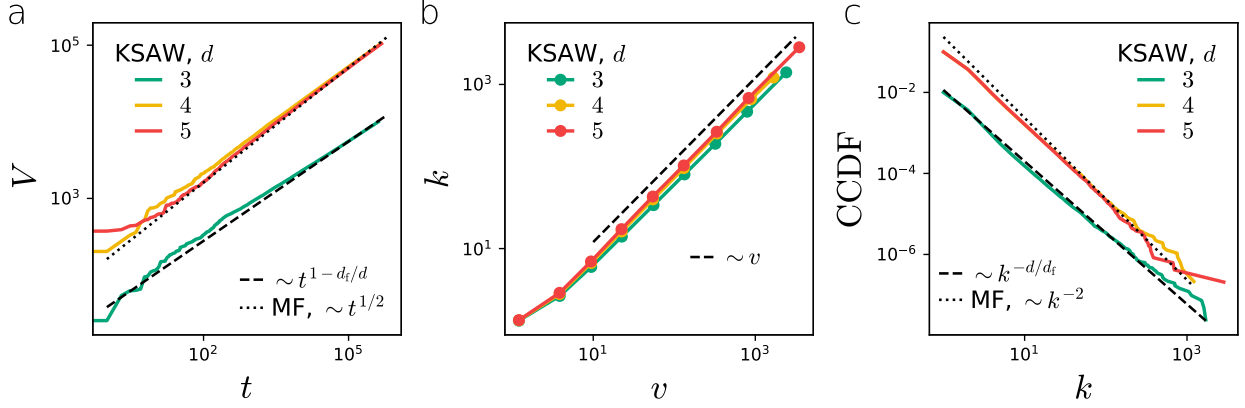


FIG. S7. **KSAW networks.** (a) Evolution of the total volume of the network V_t . (b) Correlations between node volume v and node degree degree k . (c) Complementary cumulative distribution of the node degree. (a-c) We compare the predictions of Eqs. (S1),(S2) and (S3) to numerical simulations, finding excellent agreement. The lines indicate results for a single saturated network embedded on d -dimensional square lattice with periodic boundaries and side length L , where L is chosen such that $L^d \approx 10^6$.

S1.4. Random ray

Finally, we generate random nodes tracing random rays (RR): we grow nodes from a random starting lattice site in a uniform random direction parallel to one of the axis, nodes grow until they hit an already existing node. The RR growth process produces physical nodes with $d_f = 1$ for any embedding dimension $d \leq 2$; therefore the network evolution is always in the meanfield regime. We build the networks on lattices with periodic boundary conditions, hence at the early stages of network growth, the RR trajectories often miss existing nodes, and instead return to their starting points and collide with themselves, forming rings. In these cases, we kept the trajectories in \mathcal{P} and added an isolated node to the combinatorial network \mathcal{G} ; therefore the final network breaks into many components (Fig. S8).

Figure S9 shows the physical layout \mathcal{P} and the combinatorial network \mathcal{G} of an example network generated using RRs. Figure S8 compares the analytical predictions to simulations, finding excellent agreement, with two caveats: First, for $d = 2$, the numerically measured degree distribution is in excellent agreement with the meanfield prediction (Fig. S10)c; however, the evolution of the total volume V_t and the degree-volume correlations somewhat deviate from the prediction. We explain this by the observation that for $d = 2$ long nodes can be blocked from receiving connections by other nodes running parallel to them, for example, the horizontal light blue node in Fig. S9a remains isolated due to the two parallel nodes adjacent to it. For higher embedding dimensions $d > 2$, this is an increasingly unlikely event. Second, for $d > 2$, at early stages of the network the embedding lattice is sparsely populated and nodes are likely to miss each other, This means that Eq. (1) of the main text holds only after a sufficient density of nodes is reached. This leads to a deviation from the predicted power law growth of the total volume for small t (Fig. S10a) and introduces a cutoff in the degree distribution for high k (Fig. S10c).

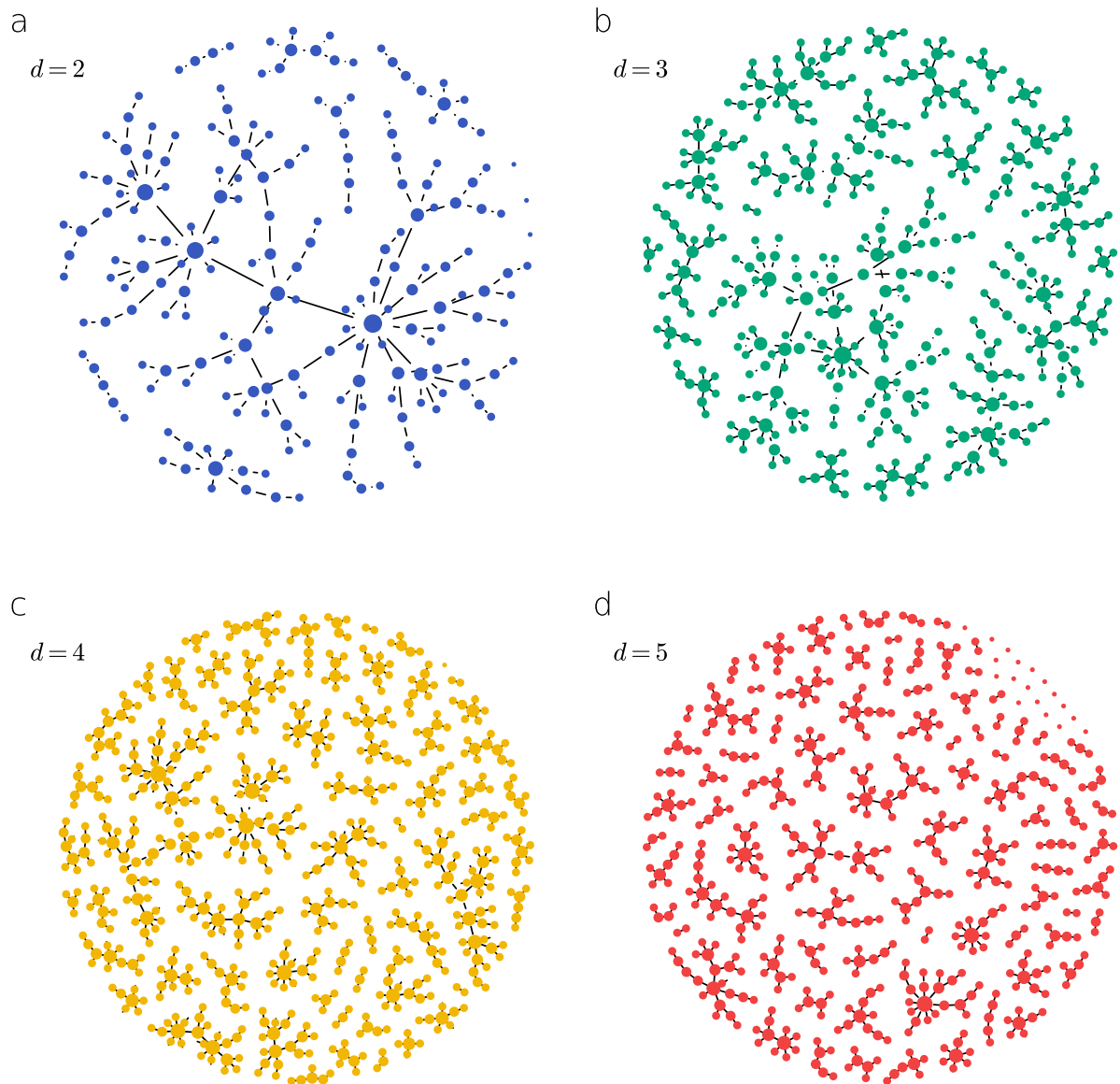


FIG. S8. **RR combinatorial networks.** (a) We show typical combinatorial networks for dimension $d = 2$, (b) $d = 3$, (c) $d = 4$ and (d) $d = 5$. (a-d) At early stages of the network evolution, node trajectories may miss other nodes and loop around to form a ring. Each of these nodes forms a connected component in the final combinatorial network \mathcal{G} . Each combinatorial network \mathcal{G} corresponds to a saturated physical layout \mathcal{P} embedded in a d -dimensional square lattice with periodic boundaries and side length L , where L is chosen such that $L^d \approx 10^3$.

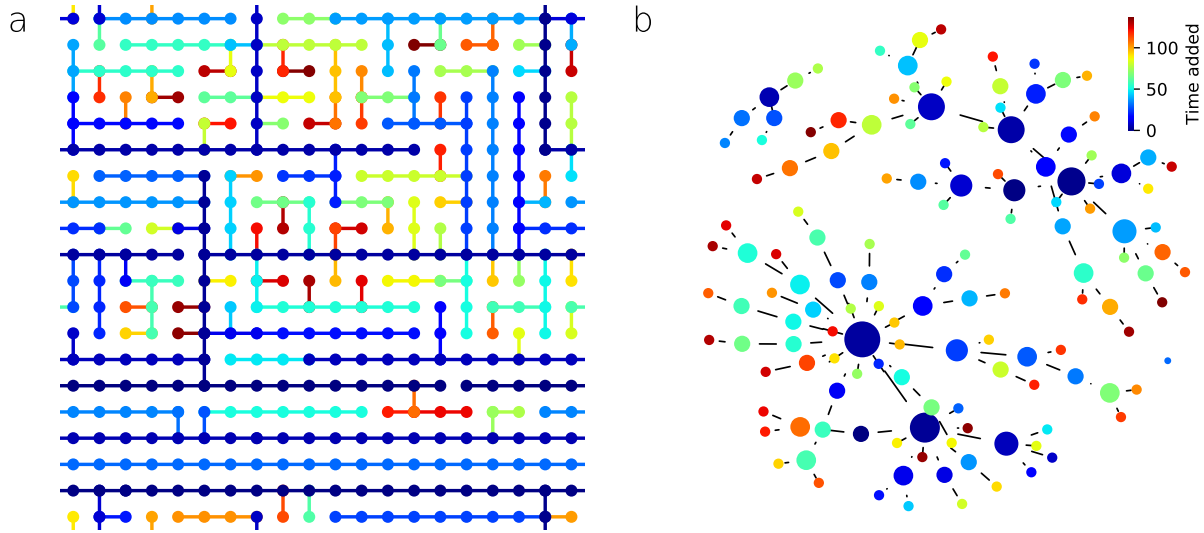


FIG. S9. **Example network generated with RRs.** (a) The physical layout \mathcal{P} of a saturated network embedded in a 20×20 square lattice with periodic boundary conditions. The color of physical nodes indicate the time they were added (note that the color of nodes added at consecutive time steps is indistinguishable). Nodes added early may loop around and form a ring. For $d = 2$, nodes with high volume may be shielded from receiving connections by adjacent nodes running parallel to them (light blue horizontal node). (b) The corresponding combinatorial network \mathcal{G} . The network has three connected components: two grown from the two horizontal dark blue nodes that form rings, and an isolated node corresponding to the light blue node shielded by its neighbors. Node sizes are a linear function of the logarithm of their degrees.

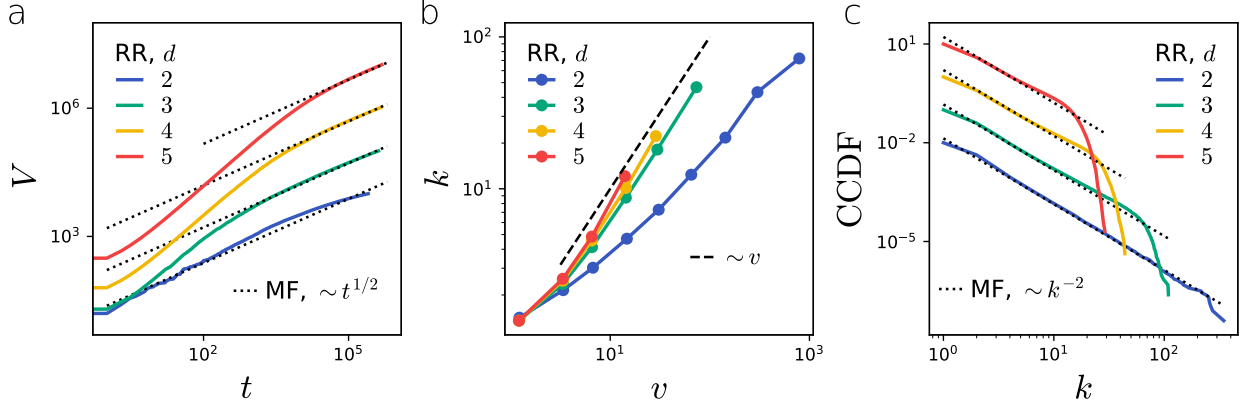


FIG. S10. **RR networks.** (a) Evolution of the total volume of the network V_t . (b) Correlations between node volume v and node degree k . (c) Complementary cumulative distribution of the node degree. (a-c) We compare the predictions of Eqs. (S1),(S2) and (S3) to numerical simulations, finding excellent agreement with two caveats:(i) for $d = 2$, the evolution of the total volume and the degree-volume correlations somewhat deviate from the prediction and (ii) for $d \leq 3$, there is an upper cutoff in the degree distribution. The lines indicate results for a single saturated network embedded on d -dimensional square lattice with periodic boundaries and side length L , where L is chosen such that $L^d \approx 10^6$.

S2. EMPIRICAL PHYSICAL NETWORKS

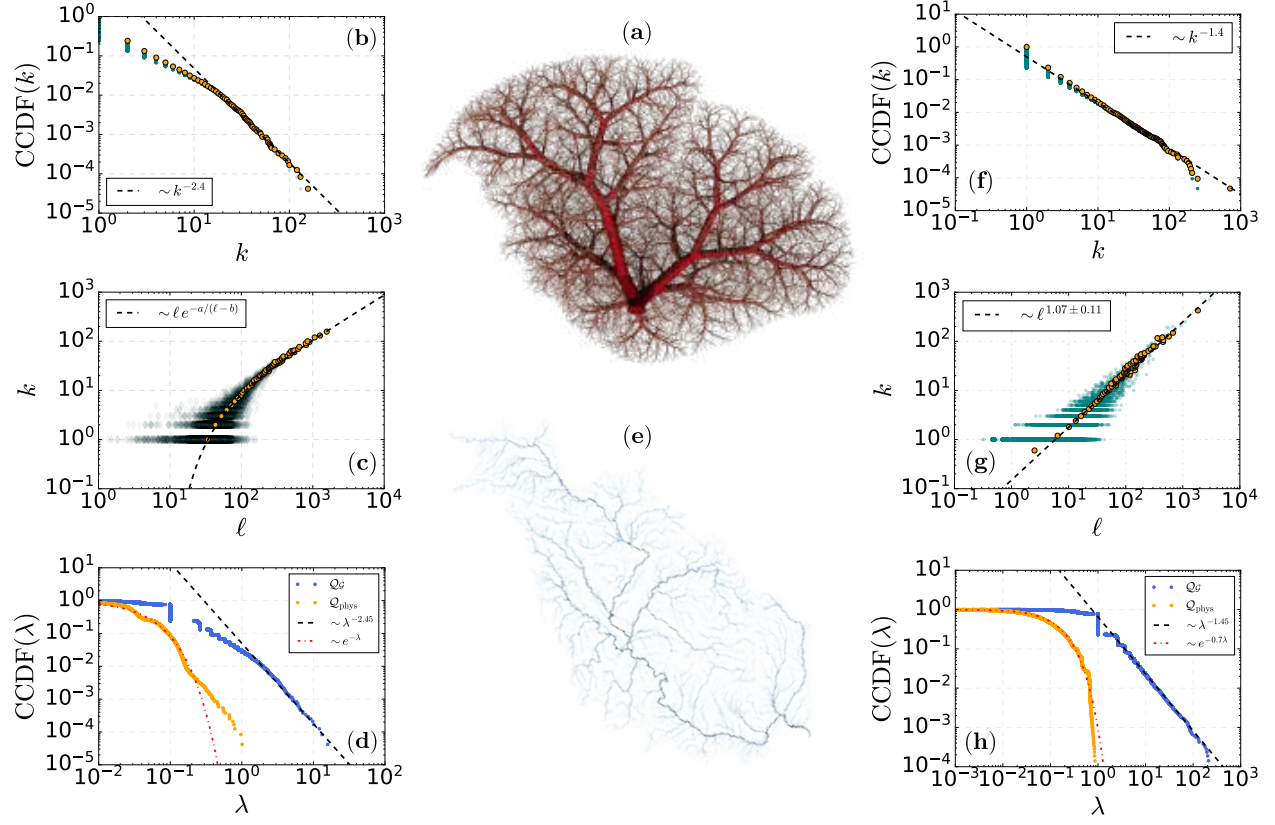


FIG. S11. **Network-of-networks analysis of real physical networks: Part I.** (a) Hepatic vascular network (HVN) generated from the corrosion cast (main sub-tree up to depth 5) of a human liver via geometric optimization [5]. The combinatorial graph, \mathcal{G} , is built following Horton’s river stream ordering scheme [6] —i.e., by labeling tributaries downstream— and it consists of $N_{\text{HVN}} = 5.9 \times 10^3$ nodes and $M_{\text{HVN}} = 5.9 \times 10^3$ edges. (b) CCDF of the degree distribution of \mathcal{G} , showing a power-law tail with exponent $\gamma_{\text{HVN}} \simeq 3.4$. (c) Linear degree-length correlation in the HVN accompanied by an exponential cut-off below $k \sim 10$ —fitted curve with $a \simeq 50$ and $b \simeq 4$ — where also the degree distribution changes trend. Given the elongated nature of physical nodes, we use lengths instead of volumes. Note that, for elongated links, positive degree-length correlation implies positive degree-volume correlations. (d) CCDF of the spectrum of the combinatorial Laplacian $\mathbf{Q}_{\mathcal{G}}$ (blue) and the physical Laplacian $\mathbf{Q}_{\text{phys}} = \mathbf{V}^{-1/2} \mathbf{Q}_{\mathcal{G}} \mathbf{V}^{-1/2}$ (orange) spectra, where the latter is obtained as in Eq. (7) in the main text, replacing volumes with lengths. Like in model networks, the spectrum of $\mathbf{Q}_{\mathcal{G}}$ exhibits a power-law tail with exponent close to γ_{HVN} , while for \mathbf{Q}_{phys} we observe a rapidly decaying spectrum. (e) Danube river network (DRN); data obtained from the HYDRORIVERS database [7]. Its combinatorial graph consists of $N_{\text{DRN}} = 2.1 \times 10^4$ nodes and $M_{\text{DRN}} = 2.1 \times 10^4$ edges, and physical nodes are labeled following Horton’s ordering scheme. (f) CCDF of the DRN degree distribution, showing a power-law tail with exponent $\gamma_{\text{DRN}} \simeq 2.4$. (g) Degree-length correlations in the DRN; best fit returns the exponent 1.07 ± 0.11 . Similar to the HVN data set, we use lengths instead of volumes. (h) CCDF of the DRN Laplacian spectrum of $\mathbf{Q}_{\mathcal{G}}$ (blue) decays as a power law, while the spectrum of \mathbf{Q}_{phys} (orange) has an exponential tail. Results similar to (a)–(d) and in (e)–(h) are found in other synthetic vascular and river networks (not shown). To calculate the spectrum of \mathbf{Q}_{phys} , we measure the volume in units such that the minimum node volume is unity, i.e., $\min_i v_i = 1$.

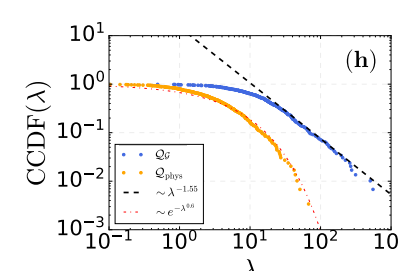
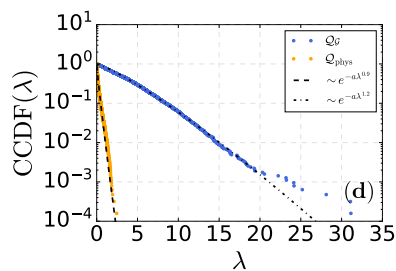
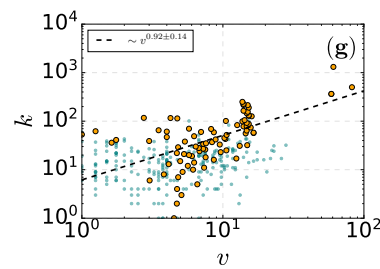
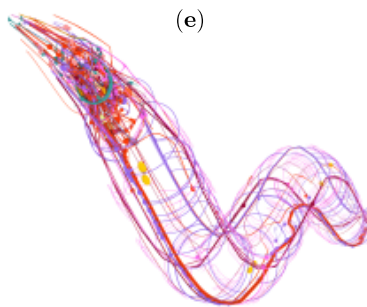
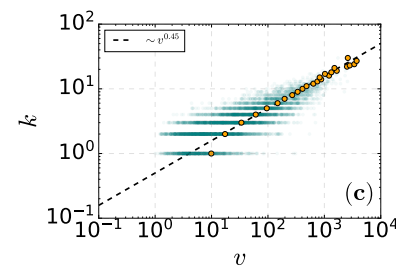
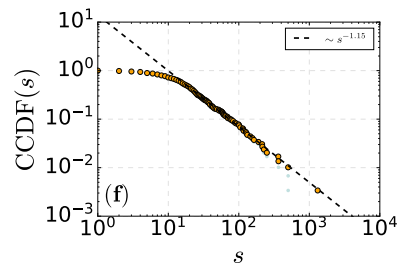
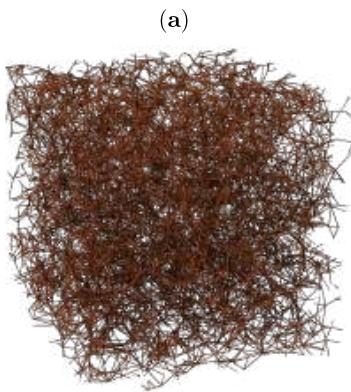
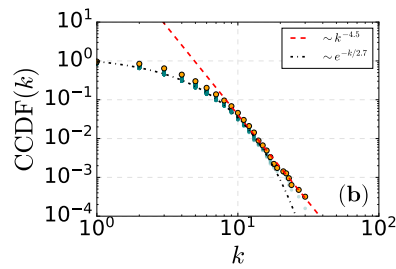


FIG. S12. **Network-of-networks analysis of physical networks: Part II.** (a) Berea sandstone porous network (SPN) [8]. In the combinatorial graph \mathcal{G} , nodes represent pores –i.e. large voids in the rock– and links model narrow pathways connecting pores, called throats [9]; here $N_{\text{SPN}} = 6 \times 10^3$ and $M_{\text{SPN}} = 1.2 \times 10^4$. (b) The number of throats are homogeneously distributed as reflected by the exponential decay of the degree CCDF. (c) We observe positive yet sublinear degree-volume correlations. (d) The CCDF of both the spectrum of $\mathbf{Q}_{\mathcal{G}}$ and \mathbf{Q}_{phys} both exhibit a stretched exponential decay due to the homogeneous degree distribution of \mathcal{G} . (e) Neural network (NN) of an adult hermaphrodite *C. elegans*; neuron size is obtained from Ref. [10] and the combinatorial graph is from Ref. [11]. The combinatorial graph takes into account only the gap junction synapses between neurons and the network is treated as undirected multi-graph, in which case $N_{\text{NN}} = 302$ and $M_{\text{NN}} = 1.1 \times 10^3$. We had to drop three neurons from the analysis because their volume was missing. (f) CCDF of the strength degree distribution of \mathcal{G} , showing a power law tail with exponent $\gamma_{\text{NN}} \simeq 2.2$. (g) Degree-volume correlations; despite that volumes are less heterogeneous than in other examples, best fit indicates a linear correlation with exponent $\alpha = 0.92 \pm 0.14$. (h) CCDF of the spectrum of $\mathbf{Q}_{\mathcal{G}}$ and \mathbf{Q}_{phys} for the *C. elegans* network. We find that spectrum of $\mathbf{Q}_{\mathcal{G}}$ has a power law tail whose exponent is in agreement with γ_{NN} and a visible exponential decay for the spectrum of spectra of \mathbf{Q}_{phys} . To calculate the spectrum of \mathbf{Q}_{phys} , we measure the volume in units such that the minimum node volume is unity, i.e., $\min_i v_i = 1$.

SUPPLEMENTARY REFERENCES

- [1] Neal Madras and Gordon Slade. *The self-avoiding walk*. Springer Science & Business Media, 2013.
- [2] Imtiaz Majid, Naeem Jan, Antonio Coniglio, and H Eugene Stanley. Kinetic growth walk: A new model for linear polymers. *Physical Review Letters*, 52(15):1257, 1984.
- [3] S Hemmer and PC Hemmer. An average self-avoiding random walk on the square lattice lasts 71 steps. *The Journal of Chemical Physics*, 81(1):584–585, 1984.
- [4] S Havlin and D Ben-Avraham. Corrections to scaling in self-avoiding walks. *Physical Review A*, 27(5):2759, 1983.
- [5] Etienne Jessen, Marc C Steinbach, Charlotte Debbaut, and Dominik Schillinger. Rigorous mathematical optimization of synthetic hepatic vascular trees. *Journal of the Royal Society Interface*, 19(191):20220087, 2022.
- [6] Amos Maritan, Andrea Rinaldo, Riccardo Rigon, Achille Giacometti, and Ignacio Rodríguez-Iturbe. Scaling laws for river networks. *Physical Review E*, 53(2):1510, 1996.
- [7] Bernhard Lehner and Günther Grill. Global river hydrography and network routing: baseline data and new approaches to study the world’s large river systems. *Hydrological Processes*, 27(15):2171–2186, 2013.
- [8] Hu Dong. *Micro-CT imaging and pore network extraction*. PhD thesis, Department of Earth Science and Engineering, Imperial College London, 2008.
- [9] Hu Dong and Martin J Blunt. Pore-network extraction from micro-computerized-tomography images. *Physical Review E*, 80(3):036307, 2009.
- [10] Balázs Szigeti, Pdraig Gleeson, Michael Vella, Sergey Khayrulin, Andrey Palyanov, Jim Hokanson, Michael Currie, Matteo Cantarelli, Giovanni Idili, and Stephen Larson. Openworm: an open-science approach to modeling caenorhabditis elegans. *Frontiers in computational neuroscience*, 8:137, 2014.
- [11] Steven J Cook, Travis A Jarrell, Christopher A Brittin, Yi Wang, Adam E Bloniarz, Maksim A Yakovlev, Ken CQ Nguyen, Leo T-H Tang, Emily A Bayer, Janet S Duerr, et al. Whole-animal connectomes of both caenorhabditis elegans sexes. *Nature*, 571(7763):63–71, 2019.